ADVANCED ELECTRONIC MATERIALS Open Access
www.advelectronicmat.de

Graphene Acetic Acid-Based Hybrid Supercapacitor and Liquid-Gated Transistor

*Rafael C. Hensel, Biagio Di Vizio, Verónica Montes-García, Jijin Yang, Georgian G. Ilie, Francesco Sedona, Mauro Sambi, Paolo Samorì, Andrea Cester, Stefano Agnoli, and Stefano Casalini**

Supercapacitors and transistors are two key devices for future electronics that must combine portability, high performance, easy scalability, etc. Graphene-related materials (GRMs) are frequently chosen as active materials for these applications given their unique physical properties that are tunable via chemical functionalization. Up to date, among GRMs, only reduced graphene oxide (rGO) showed sufficient versatility and processability in mild media, rendering it suitable for integration in these two types of devices. Here, a sound alternative to rGO is provided, namely graphene acetic acid (GAA), whose physico-chemical features offer specific advantages. In particular, the use of a GAA-based cathode in a zinc hybrid supercapacitor (Zn-HSC) delivers state-of-the-art gravimetric capacitance of ≈400 F g^{-1} at a current density of 0.05 A g^{-1}. Conversely, GAA-based LGT, supported onto Si/SiO_2, shows an ambipolar behavior in 0.1 M NaCl, featuring a clear p-doping quantified by Dirac voltage higher than 100 mV. Such a device is successfully implemented in paper fluidics, thereby demonstrating the feasibility of real-time monitoring.

1. Introduction

The discovery of graphene's exceptional mechanical, electrical, thermal, and optical properties[1–4] has fuelled an extensive research effort towards technological applications in drug delivery,[5] sensing,[6,7] energy storage,[8] and electronics.[9] Although graphene shows exceptional features, its processability due to restacking/agglomeration of the flakes and zero bandgap limits the final performance of graphene-based devices.[10,11] The chemical functionalization of graphene played a key role in addressing these open challenges because its derivatization can improve water dispersibility and even tune its electronic conductivity.[12–17] One of the most popular examples of chemical modification of graphene is graphene oxide (GO), whose backbone bears many oxygen groups (viz. hydroxyl, carboxyl, epoxide, carbonyl, etc.) due to its extensive oxidation.[18,19] This massive chemical modification determines an abrupt loss of conductivity (i.e., GO is an insulator), but it gains ideal water dispersibility due to the high density of hydrophilic groups. Many physical and chemical processes allow a partial restoration of the sp2-hybridized carbons, which are responsible for the high conductivity of graphene, thereby leading to reduced graphene oxide (rGO).[20–27] Apart from GO and rGO, there are further routes to synthesize relevant graphene-related materials (GRMs), such as fluorographene (FG).[28] In terms of sustainability, fluorographite is extremely convenient (viz. it is used as a lubricant, so it is massively produced by companies).[29] FG affords the synthesis of stoichiometric graphene derivatives such as graphene acid (GA) compared to the ill-defined stoichiometry of GO/rGO, which does not allow proper control of its chemical functionalization.[30,31]

These GRMs offered scientists a materials platform for energy storage devices and transistors due to their promising features such as physico-chemical robustness and electrical conductivity. Concerning supercapacitors, there are different high-performing supercapacitors (i.e., gravimetric capacitance > 300 F g^{-1}), whose performances rely on GO[32,33] and FG functionalized by hydrophilic/zwitterion groups[34] as well as pristine rGO.[35] The exploitation of hydrophilic/zwitterion groups such as thioamide,[33] arginine,[34] tri(hydroxymethyl)aminomethane,[32] etc. favors

R. C. Hensel, B. Di Vizio, J. Yang, G. G. Ilie, F. Sedona, M. Sambi, S. Agnoli, S. Casalini
Department of Chemical Sciences
University of Padua
Via Francesco Marzolo, 1, Padua 35131, Italy
E-mail: stefano.casalini@unipd.it
R. C. Hensel
São Carlos Institute of Physics
University of São Paulo
Av. Trab. São Carlense, 400, São Carlos 13566-590, Brazil
V. Montes-García, G. G. Ilie, P. Samorì
CNRS
ISIS UMR 7006
Université de Strasbourg
8 allée Gaspard Monge, Strasbourg F-67000, France
A. Cester
Department of Information Engineering
University of Padua
Via Giovanni Gradenigo, 6b, Padua 35131, Italy

The ORCID identification number(s) for the author(s) of this article can be found under https://doi.org/10.1002/aelm.202300685

DOI: 10.1002/aelm.202300685

efficient trafficking of ions inward/outward the bulk of the supercapacitor, whereas the pristine rGO[35] takes advantage of its ill-defined stoichiometry along with the high content of defects, and a satisfactory conductivity. Regarding transistors, some of the GRMs as FG, and GO are not well-suited because of their insulating features. The sole example consists of using rGO, whose conductivity and water dispersibility satisfy the basic requirement to fabricate and operate transistors. Moreover, the fabrication of liquid-gated transistors (LGTs) takes advantage of the aqueous solution as gate dielectric, and this allows them to be operated at low operational voltages (i.e., <1 V).[36] The working principle stems from the formation of two electrical double layers (EDLs), one placed at the interface between the gate terminal and the electrolyte and the second one at the interface between the active material and the electrolyte.[37] The research group led by W. Knoll demonstrated the best rGO-based LGT (viz. mobility equal to 10^4 $cm^2V^{-1}s^{-1}$), and this technology allowed the development of different types of sensors, e.g., pH, bovine serum albumin, urea, and Cu^{2+} ions.[38,39] Despite these excellent results, such devices needed hydrazine vapors to achieve the proper GO reduction, hence their manufacturing poses severe problems in terms of sustainability and throughput. According to these limitations, an alternative and green approach has been developed by means of electrochemical reduction. Although the performances of these LGTs are orders of magnitude lower than the previous devices (i.e., 10^{-1} $cm^2V^{-1}s^{-1}$), they have been successfully exploited as both sensors (i.e., analytes detected: cations and anti-drug antibodies) and transducers (viz. mechanical stress, change of ionic strength and emulated action potentials).[26,40–44]

Among GRMs, only rGO can be implemented in both supercapacitors and LGTs. For these reasons, we decided to provide an alternative candidate. Since such a candidate must be conductive and easily processable, we focused our attention on graphene acid (GA) which satisfies these mandatory requirements. To the best of our knowledge, GA shows poorer gravimetric capacitances (i.e., 40–90 F g^{-1}) than the best-performing GRMs-based supercapacitors,[31,45] and no evidence for its implementation in transistor-s. For these reasons, we decided to synthesize graphene acetic acid (GAA), whose synthesis is more sustainable and safer than GA because it relies on an eco-friendly nucleophilic agent, namely diethyl malonate, which replaces the more harmful cyanide. GAA differs from GA by an additional methylene unit (—CH_2—) that acts as a spacer between the carboxylic groups (viz. —COOH) and the sp^2-hybridized C basal plane. Although —CH_2— represents a subtle difference compared to pristine GA, the —COOH groups benefit from better exposure to the solvent yielding boosted water dispersibility. Furthermore, GAA nanosheets benefit from an intrinsically increased interlayer distance due to the presence of this methylene unit (viz. —CH_2— means roughly 1.5 Å) with respect to GA ones. Finally, the GAA implementation in LGT architecture makes it more straightforward in the overall manufacturing, since no reduction steps are required like for rGO. This aspect plays a fundamental role in the early-stage development of a new technology facilitating its scale-up.

Besides a multi-methodological characterization of the GAA focused on morphology, surface charges, and elemental mapping, we first evaluated the performance of GAA in two electrochemical systems: i) a symmetric one and ii) zinc hybrid supercapacitors (Zn-HSC), in both of which it revealed state-of-the-art performance (viz. up to 400 F g^{-1}). These promising achievements allowed us to exploit the GAA conductivity along with its energy storage capability to fabricate liquid-gated transistors (LGTs).[46] Regarding the LGT fabrication, GAA is cast on top of both working interfaces and this device exhibits clear ambipolar behavior, like the graphene-based ones.[47,48] As a result, the operating potential range spans from −300 mV to 300 mV, whereas a marked p-doping is registered due to the wealth of oxygen groups in the GAA backbone. This performance is similar to the rGO-based LGT fabricated by using electrochemical reduction. Our research also confirmed the GAA-based LGT's ability to monitor 0.1 M NaCl flux in real-time for at least an hour, maintaining its potentiometric sensitivity for both p- and n-type conduction. These outcomes suggest that not only rGO can be implemented in supercapacitors and LGTs, but also GAA shows similar versatility and performances. Conversely to rGO, GAA shows specific advantages such as a well-defined stoichiometry, a more sustainable synthesis, and a more straightforward fabrication of LGT, paving the way towards a promising scaling up of this technology.

2. Results and Discussion

The GAA was prepared through a more sustainable synthesis compared to that employed for GA,[30] which relies on the nucleophilic substitution of the fluorine of fluorinated graphite with the diethyl malonate group, as shown in **Figure 1**. See more details in the experimental section.

The replacement of potassium cyanide (KCN) with diethyl malonate group not only improves sustainability and safety but also GAA throughput. As a result, many safety issues are avoided by using this affordable reagent, which allows an unlimited production of GAA compared to the synthesis based on KCN according to the Italian safety regulations applied to our laboratories. Furthermore, the price of diethyl malonate is six times lower than KCN, hence the synthesis is far cheaper than the one based on KCN.

A multi-methodological characterization has been performed, which relies on transmission electron microscopy (TEM), thermal gravimetry analysis (TGA), Fourier transform infrared spectroscopy (FT-IR), Raman spectroscopy, X-ray diffraction (XRD), X-ray photoelectron spectroscopy (Figures S1-S6 and Table S1, Supporting Information). Morphological and elemental characterizations show that GAA retains the main chemico-physical features of GA (more details in the Supporting Information). For instance, morphology shows single GAA nanosheets featuring 100–300 nm sizes, whereas XPS highlights a ratio of 6:1 of C sp^2 with respect to -COOH and Raman spectroscopy evidences a ratio between G and D bands corresponding to 1.03.

In view of such interesting properties, we have focussed our attention on two different types of functional applications, i.e., supercapacitors and LGTs. Within this context, technological advancements require the investigation of suitable and efficient electrode/electrolyte materials to optimize energy storage, power density, cyclability, and safe operation. The comprehensive investigation of the GAA towards an efficient supercapacitor has been crucial for achieving a working LGT, whose layout exploits two GAA-based coatings, namely one onto the gate terminal and

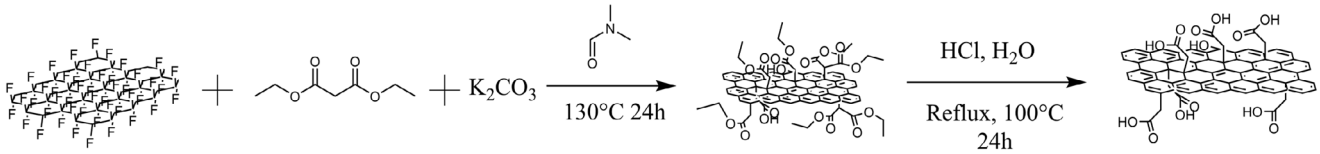

Figure 1. Scheme of the synthetic route for GAA.

another one onto the interdigitated electrodes (IDEs). To the best of our knowledge, only rGO has been successfully implemented in both supercapacitors and LGTs among the wide library of GRMs.

2.1. Electrochemical Performance of GAA-Based Supercapacitors

The electrochemical performance of GAA is first assessed in a symmetrical two-electrode cell by cyclic voltammetry (CV) and galvanostatic charge/discharge (GCD), as shown in Figure S7 (Supporting Information). Since the maximum gravimetric capacitance amounts to 75.4 F g^{-1} at 0.25 A g^{-1} and a capacitive decrease of less than 7% at higher current densities, we decided to implement GAA in a more technologically relevant system, namely aqueous Zn-HSCs, wherein a single electrode with a mass loading of ≈1 mg is assembled in a coin-type cell with a Zn anode by using zinc trifluoromethanesulfonate, $Zn(OTf)_2$, as electrolyte. **Figure** 2a–c shows the CV and GCD curves of GAA in a potential range within 0 and 1.8 V and at different scan rates from 10 to 200 mV s^{-1} or current densities from 0.05 to 1 A g^{-1}, respectively. In analogy to the symmetric configuration, the CV curves of GAA display a typical quasi-rectangular shape and the GCD curves show a distorted triangular shape, both being characteristic of pseudocapacitors. Subsequently, the gravimetric capacitance of GAA is calculated from the GCD analysis between the adopted potential window, revealing that the GAA cathode displays a state-of-the-art gravimetric capacitance as high as ≈400 F g^{-1} at the current density of 0.05 A g^{-1} (Figure 2d). The excellent performance of GAA electrodes can be attributed to their remarkable physico-chemical characteristics, high electrical conductivity (12 ± 1 S m^{-1}), ionic conductivity (35.2 ± 0.2 mS m^{-1}), and the presence of —COOH groups, whose hydrophilicity make more efficient the ions trafficking (see Experimental Section for details). A good rate capability is achieved for GAA, where a gravimetric capacitance value of 214.4 F g^{-1} is still obtained at a current density of 1 A g^{-1}. Furthermore, GAA exhibits an outstanding maximum energy density of 104 Wh kg^{-1} and a maximum power density of 2.03 kW kg^{-1}, with a coulombic efficiency of nearly 100%. The prolonged charge and discharge test (Figure 2e) provides evidence for the high cyclability of GAA cathodes at a high current density of 1 A g^{-1}, which can retain ≈94% of the initial capacity value after >2000 cycles. Moreover, the electrochemical impedance spectroscopy (EIS) data are shown in the Nyquist plot (Figure 2f). The Nyquist plot contains a semicircle with an offset from the origin on the x-axis. Such offset corresponds to the resistance R_s, which include internal resistances, interfacial contact resistance of the materials with the current collector, and wires.[49,50] R_{ct} is the interfacial charge transfer resistance, corresponding to the diameter of the semicircle, which represents the resistance of electrochemical reactions at the electrode surface.[51] To determine these values, a fit has been achieved by an equivalent circuit composed of the following parameters: R_s, R_{ct}, C is the geometric capacitance, CPE_{EDL} is the constant phase element representing the electrical double-layer capacitance (EDLC = $Y_{\mathrm{CPE}} \times \omega_{\mathrm{MAX}}^{n_{\mathrm{CPE}}-1}$) as a function of Y_{CPE} (viz. admittance) and n_{CPE} (viz. exponent related to the admittance), ω_{MAX} is the angular frequency for the maximum imaginary impedance.[52] Although the R_{ct} value of GAA is similar or higher compared to other devices (Table S2, Supporting Information), this does not affect the gravimetric capacitance of our supercapacitor (fixed current density 1 A g^{-1}), indicating a good rate capability of the GAA sample. According to the literature on supercapacitors, the gravimetric capacitance value is only outperformed by GO functionalized by tris(hydroxymethyl)aminomethane,[32] and a few other GRMs such as rGO[35] and FG functionalized by 5-aminoisophthalic acid[53] show similar values. The presence of the hydrophilic group (—COOH) spaced by one methylene unit from the basal plane yields a gravimetric capacitance increase of one order of magnitude with respect to GA, hence GAA shows a slightly better performance compared to pristine rGO (i.e., 400 F g^{-1} versus 370.8 F g^{-1}), whose synthesis requires high power approaches to achieve the proper grade of reduction (see Table S3, Supporting Information, for a more detailed comparison between GAA figure of merits and other GRMs).

2.2. Preparation and Characterization of GAA-Based LGTs

Concerning the LGT fabrication, the three terminals have been photolithographically manufactured onto Si/SiO_2 chips. The LGT layout consists of IDEs (i.e., source and drain, electrodes) and a coplanar and square gate electrode (**Figure** 3a). Furthermore, such a device relies on two GAA-based coatings: the former cast onto the IDEs and the latter onto the gate electrode (more details are provided in the experimental section). The former acts as the active material of the LGT, whereas the latter must improve the gate efficiency by increasing its capacitance.[42] Aiming at these two crucial aspects of the transistor, two different GAA solutions have been exploited as follows: i) 5 mg mL^{-1} featuring an acidic pH related to the GAA cast onto the gate and ii) 1 mg mL^{-1} at alkaline pH corresponding to the GAA cast onto the channel. The former GAA solution yields rougher and thicker GAA coating since its concentration and pH favor a partial GAA agglomeration.[30,54] On the contrary, the latter affords better control of the GAA coating morphology (pH-dependency analysis by tracking the ζ-potential reported in Table S4, Supporting Information).[30] As a result, the SEM micrographs of the GAA onto the IDE and the gate confirm a clear morphological difference (Figure 3b–e), with the former being smoother and more compact than the latter. The thickness of both coatings was

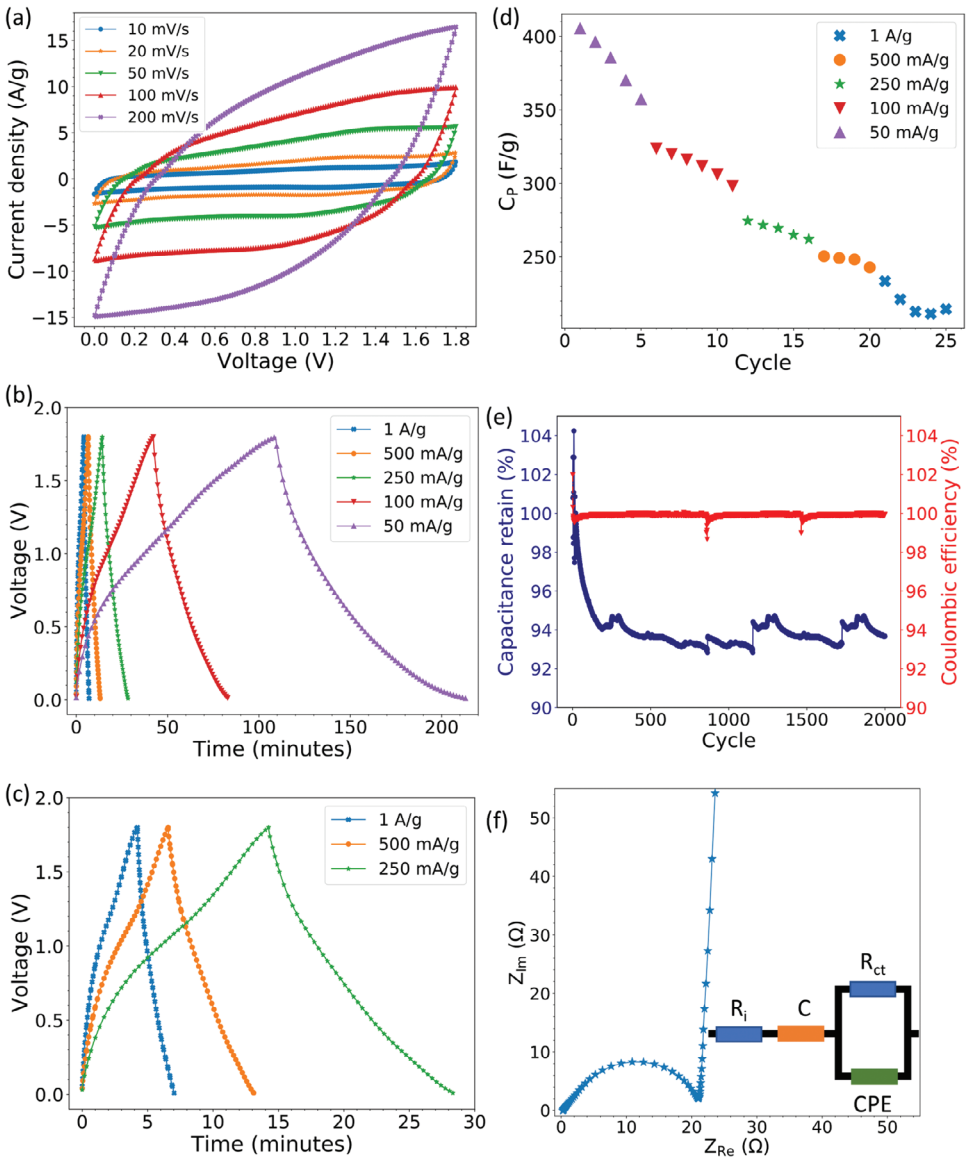

Figure 2. Electrochemical characterization of GAA as Zn-HSCs. a) CV curves at different scan rates. b-c) overlay of the whole series of GCDs and a magnification of the highest current densities and d) Gravimetric capacitances at different current densities. e) Cycling stability at 1A g^{-1}. f) Nyquist plot (e-inset) the equivalent electric circuit model used for fitting the Nyquist plots. *Rs* = 274 mΩ, *Rct* = 22.4 Ω, *C* = 29.4 mF, Y_{CPE} = 365 S, and n_{CPE} = 0.705.

determined by a profilometer (Figure S8, Supporting Information). These profiles indicate that the GAA thickness on the gate and the channel correspond to 5(± 1) µm and 1.0(± 0.2) µm, respectively. Unfortunately, GAA shows poor adhesion, hence we encounter severe difficulties in operating the GAA-based device in aqueous solutions due to its extensive detachment. For this reason, a layer of Nafion was spin-coated onto the deposited GAA, which acts as both a physical barrier to strengthen GAA coatings, and an electrostatic shield towards harmful anions such as chloride (i.e., Cl^- anions are complexing agents towards Au, hence their presence makes the Au oxidation and delamination easier). Furthermore, it has been already demonstrated that covering (semi-)conducting materials with Nafion does not affect their electronic features.[55–57]

We investigated the intrinsic conductivity of the deposited GAA by means of I-V characterization. **Figure** 4a shows the ohmic behavior of the GAA coating onto the IDEs in the air, resulting in a conductivity of 1.819(±0.001) mS m^{-1}.[58] The *I–V* transfer characteristics of the GAA-based LGT were investigated in MilliQ water and NaCl 0.1 M, since the former allows the least electrical stress and preliminary proof of feasibility validation, whereas the latter enables a more comprehensive characterization in terms of stability and possible interferences due to high ionic strength. Our GAA-based LGT shows a marked hysteresis when operated in MilliQ water (results not shown), but its performance is improved by using 0.1 M NaCl, which confers a higher ionic conductivity to the aqueous solution (Figure 4b and Figure S9, Supporting Information). This significant

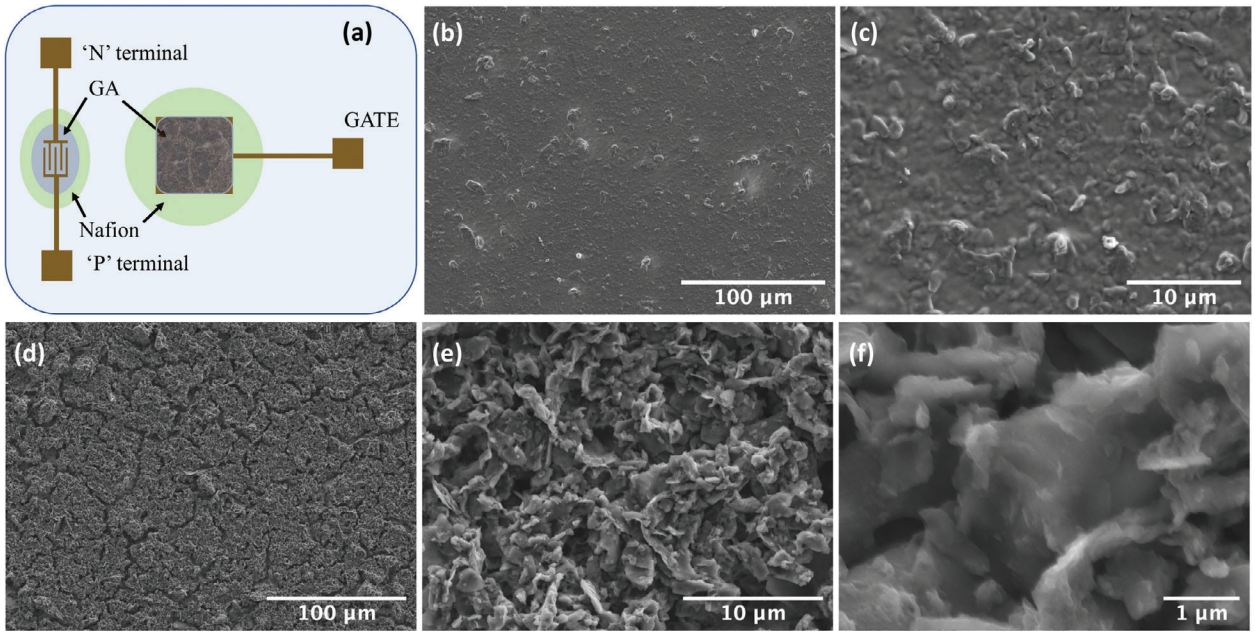

Figure 3. a) Top view of the device sketch illustrating the GAA and Nafion layers onto the gate and the channel, respectively. SEM micrographs of the GAA deposited onto the b,c) channel and d–f) gate.

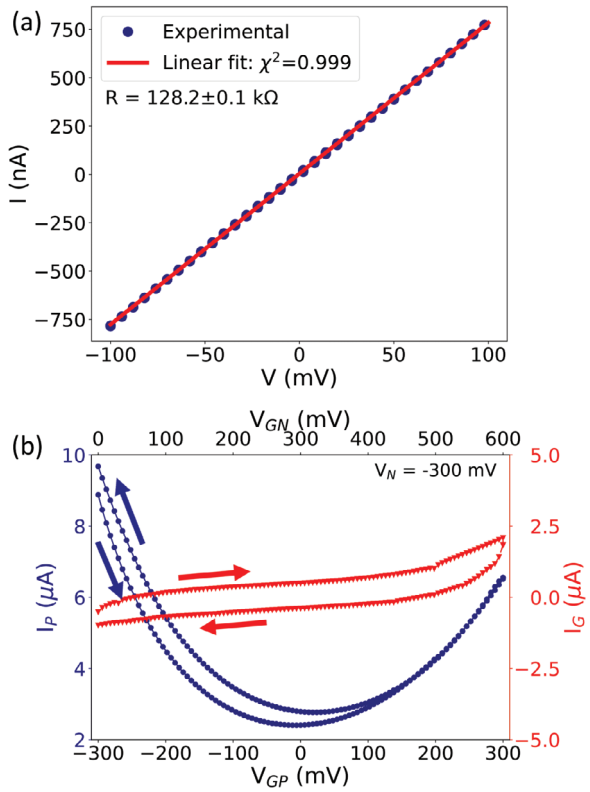

Figure 4. a) *I–V* measurement of the GA layer onto channel recorded in the air. b) *I–V* transfer characteristics of GAA-based device featuring GAA-coated Au gate recorded in 0.1 M NaCl. The blue curve stands for the current recorded at the P terminal (I_P), and the red one stands for the leakage current (I_G). V_P = 0 V and V_N = −300 mV; V_{GP} and V_{GN} = (V_G − V_N) ranges are presented as the bottom and top *x*-axis, respectively.

improvement can be ascribed to more efficient EDLs that are responsible for the electrostatic coupling of the gate terminal with the GAA-based film.[59,60] The electrical characterization is performed by exploiting the convention introduced by Lago et al., where the positive and negative electrodes (i.e., corresponding to the source and drain terminals of the standard convention) act as sources of holes and electrons, respectively.[43,61] The *I–V* transfer shows a clear ambipolarity in 0.1 M NaCl, in which V_N = −300 mV, and the gate voltage (V_{GP} = V_G − V_P) was swept from −300 mV to +300 mV, fixing a scan rate to 40 mV s^{-1}. This behavior is similar to graphene- and rGO-based transistors.[41,62–64] Indeed, in comparison to rGO-based LGTs, we observe an improvement in the conduction of electrons/holes, indicated by a clear parabolic profile centered around V_{GP} = 0 V.[40,65] We use the equations that describe ambipolar transistors to calculate the mobility and threshold voltages of holes (μ_h, $V_{th,P}$) and electrons (μ_e, $V_{th,N}$) from the *I–V* transfer curve.[43,61,66] The obtained values among the calculated minimum gate voltage ($V_{G,MIN}$) and Dirac voltage (V_{DIRAC})[67] are presented in **Table 1**. Note that the obtained (V_{TP} + V_P) and (V_{TN} + V_N) values indicate that the left- and right-hand side of the parabola refer to the p-type and n-type unipolar region, respectively. Although the parabolic shape is centered at V_{GP} = 0 V, the GAA is p-doped since V_{DIRAC} > 100 mV and the potential range of V_{GN} is mainly focused on the injection of electrons (i.e., 0 V < V_{GN} < 600 mV), as shown in Figure 4b. Regarding the obtained field-effect mobility, both μ_h and μ_e presented values equivalent to those reported for electrochemically reduced GO-based LGT,[26,40–43] and lower than rGO-based LGT in which GO was reduced by exploiting hydrazine and thermal heating, (viz. mobility equal to 10^4 cm^2 V^{-1} s^{-1}).[38,39] As a result, the advantage of using GAA compared to rGO, apart from the previous considerations related to supercapacitors consists of developing a more

Table 1. Threshold voltage for holes ($V_{Th,P}$) and electrons ($V_{Th,N}$), the minimum gate voltage ($V_{G,MIN}$), Dirac voltage (V_{DIRAC}) mobility of holes (μ_h), and electrons (μ_e) calculated according to the data shown in Figure 4.

	$V_{Th,P}$ [mV]	$V_{Th,N}$ [mV]	$V_{G,MIN}$[67] [mV]	V_{DIRAC}[67] [mV]	μ_P [cm^2 V^{-1} s^{-1}]	μ_N [cm^2 V^{-1} s^{-1}]
Forward	11 ± 2	287 ± 1	6 ± 1	149 ± 1	0.152 ± 0.004	0.041 ± 0.001
Backward	44 ± 2	313 ± 1	36 ± 1	179 ± 1	0.141 ± 0.001	0.047 ± 0.001

straightforward fabrication, which leads to an easier scaling up and device throughput.

2.3. Investigation of GAA-Based LGT Transient Phenomena

Apart from the quasi-static measurements, we performed additional investigations to explore transient phenomena, including response time and potentiometric sensitivity.

The response time and potentiometric sensitivity of GAA-based LGTs are characterized by monitoring the current I_P over time in response to gate voltage pulses (V_{GP}) of different magnitudes, using 0.1 M NaCl as an electrolyte. Our results (**Figures 5a** and S10a, Supporting Information) show that switching the gate voltage from the point of minimum to the one of maximum transconductance for electrons and holes, respectively, causes a steep increase in the I_P current followed by a decay that tends to stabilize after one minute. The I_P behavior was fitted according to Equation (1).

$$I\ (t) = A + B \times \exp\left(-\frac{t}{\tau_1}\right) - C \times \exp\left(-\frac{t}{\tau_2}\right) \quad (1)$$

in which A, B, C, τ_1, and τ_2 are functions of resistances, capacitances, steady-state drain current, gate voltage, and transconductance, according to the equivalent circuit proposed elsewhere.[68] Equation (1) models the charging behavior of the LGT active material and of the Nafion membrane cast on top by means of two time constants τ_1 and τ_2, respectively. By fitting the experimental data to Equation (1), we obtained $\tau_1 = 34 \pm 1$ s and $\tau_2 = 0.25 \pm 0.01$ s, and $\tau_1 = 29 \pm 1$ s and $\tau_2 = 0.12 \pm 0.01$ s for the n- (Figure 5a) and p-type (Figure S10a, Supporting Information) GAA-based LGT operation, respectively. Moreover, the potentiometric sensitivity (Figure 5b and Figure S10b, Supporting Information) indicates that the lowest V_{GP} step that provides a recordable change on I_P was 3 mV with a signal-to-noise ratio (SNR) of 5 and 12 for both n- and p-type branches, respectively.

2.4. Response to Prolonged Electrical Stress

Aiming at real-time monitoring of specific events occurring in aqueous solution, we challenge our GAA-based LGTs to prolonged electrical monitoring of 0.1 M NaCl flux through paper fluidics. **Figure 6a** shows that we can operate successfully the LGT up to 1 h exploiting n-type conduction. Moreover, I_P and I_G decrease over time until stabilizing at 2.3 μA and 69 nA, respectively. A fingerprint of stable functioning is the fact that I_G is almost two orders of magnitude lower than I_P. Furthermore, this is corroborated by the potentiometric sensitivity evaluation after the prolonged stress (Figure 6b), which maintains the lowest recordable $\Delta V_G = 3$ mV. Similar behavior is obtained for the device operated in p-type as shown in Figure S11 (Supporting Information).

3. Conclusion

In this paper, we successfully synthesize GAA, whose chemical backbone differs from GA by an additional methylene unit between the —COOH group and the C sp^2 basal plane, thus offering an increased spacing of the GAA nanosheets along with better exposure of the —COOH groups, which are pivotal for further chemical functionalization. This novel graphene derivative is implemented for the first time in supercapacitors and LGTs. To achieve these goals, we exploit two fundamental features of the GAA, namely its ionic conductivity as high as 35.2 ± 0.2 mS m^{-1}, along with its excellent gravimetric capacitance (≈400 F g^{-1} in a Zn-HSC configuration for a current density of 0.05 A g^{-1}, retaining ≈94%, of the initial capacity value after >2000 cycles even at a high current density of 1 A g^{-1}.). The energy storage behavior of GAA allows us to fabricate an LGT by using the GAA as both a primer to the gate electrode and as the active material bridging the positive (viz. source of holes) and negative (viz. source of electrons) terminals. A Nafion membrane provides a more robust architecture in terms of GAA adhesion as well as electronic tuning. As a result, quasi-static measurements highlight a p-doping of the GAA since $V_{DIRAC} > 100$ mV. Furthermore, such a device shows a potentiometric sensitivity down to 3 mV, and a response time lower than 1 s for both conduction branches. This device can be operated for a prolonged time (i.e., >1 h) in a media having ionic strength comparable to real matrixes such as tap water, seawater, or biological fluids. To the best of our knowledge, only rGO showed satisfactory versatility to be implemented in both supercapacitors and LGTs. Here, we provide an alternative material for these purposes that offers similar performances but additionally well-defined advantages in terms of sustainability and device throughput.

4. Experimental Section

Materials: Poly(diallylammonium chloride) (PDDA), separators, Whatman glass microfiber filters, binder poly(tetrafluoroethylene), fluorographite, diethylmalonate, potassium carbonate, dimethylformamide (DMF), hydrochloric acid (HCl), and 1-methyl-2-pyrrolidinone were purchased from Sigma–Aldrich. Conductive Carbon Black Super P (H30253) was acquired from Alfa Aesar and carbon AvCarb P75 substrate was gained from FuelCellStore.

GA Synthesis: As described in ref. [30], the GA synthesis relies on the following procedure. Fluorinated graphite (120 mg, ≈4 mmol of C-F units) was added to 15 mL of DMF and sonicated for 4 h under a nitrogen atmosphere in a 25 mL round-bottom glass flask. Then 800 mg of NaCN was added and the mixture was heated at 130 °C with a condenser under stirring. The materials were then separated by centrifugation and further purified by successive washing steps using DMF, dichloromethane, acetone,

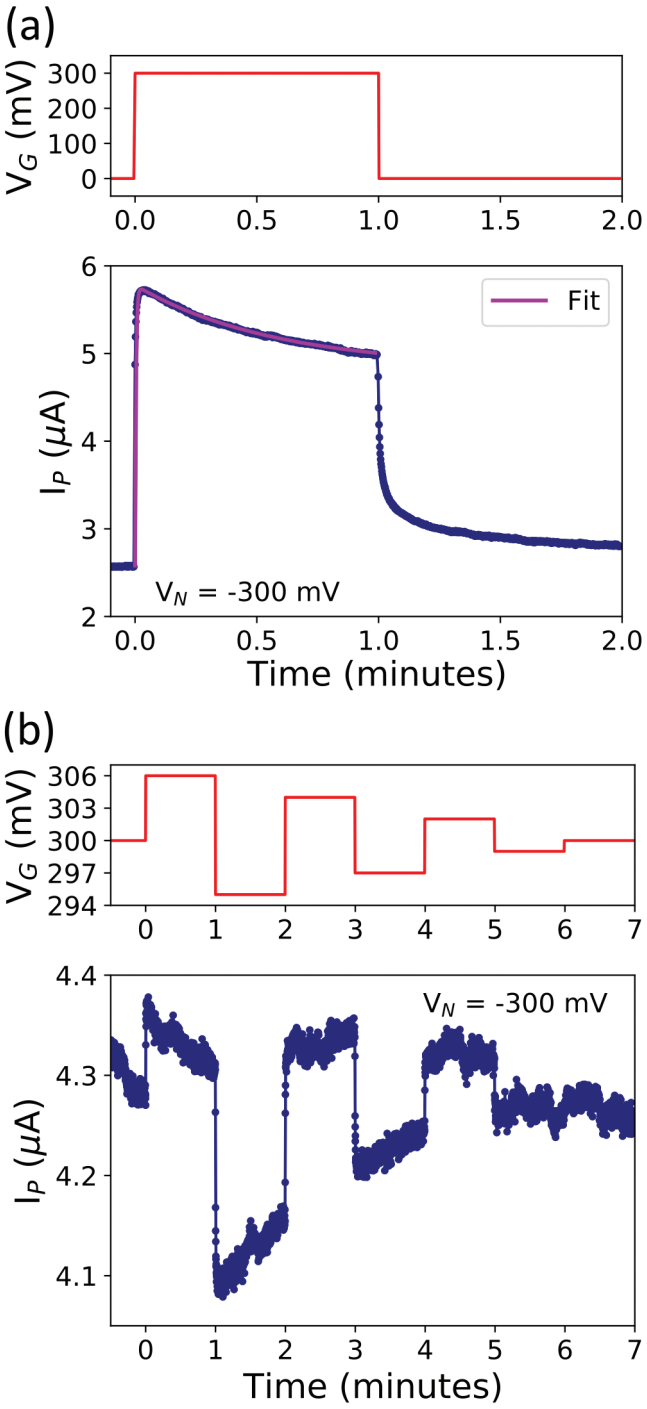

Figure 5. a) Response time (magenta solid line represents the fit), b) potentiometric sensitivity of the GAA-based LGT in 0.1 M NaCl for n-type conduction.

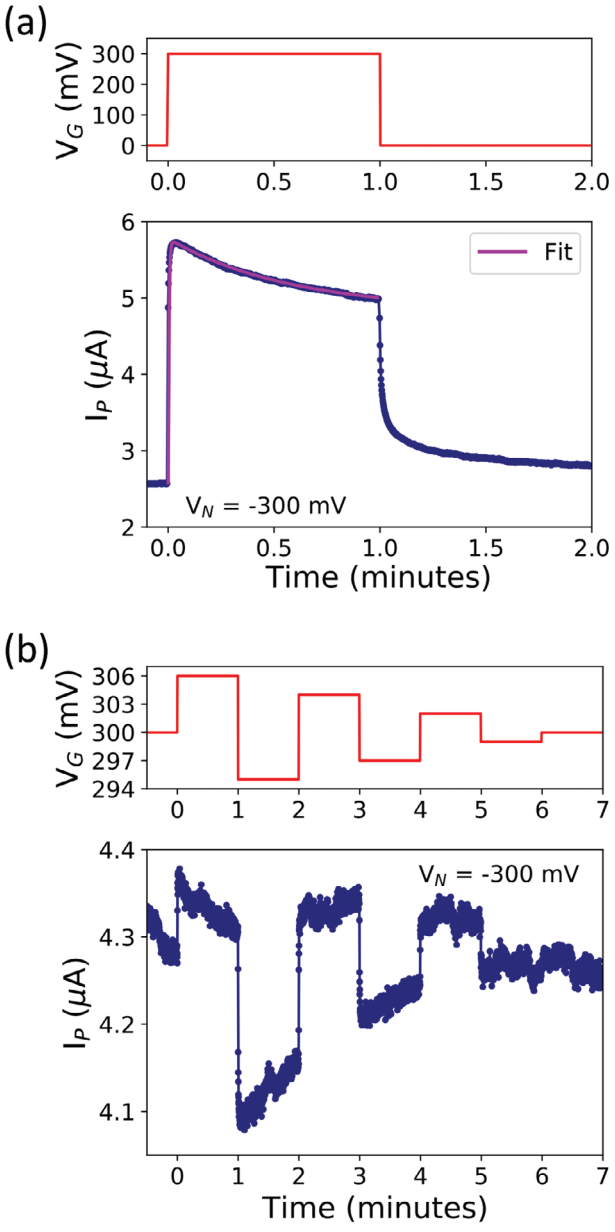

Figure 6. a) I_G and I_P versus time plots for the prolonged electrical stress investigation, in which $V_N = -300$ mV, $V_P = 0$ V, and $V_G = +250$ mV were fixed. b) Potentiometric sensitivity of the GAA-based LGT after the stress measurements. Both measurements were recorded in 0.1 M NaCl flux exploiting paper fluidics.

ethanol, and water (all 4×). Hot (80 °C) DMF and water were also used. HNO_3 (65%) was slowly added at RT under stirring to a suspension of step 1 material in water in a round-bottom glass flask until the final concentration of HNO_3 in the mixture reached 20%. The mixture was then heated at 100 °C under reflux with stirring for 24 h. Purified by washing with water through centrifugation.

GAA Synthesis: 7.5 mL of DMF was introduced in a Kolben flask under an inert atmosphere and purified by three vacuum/nitrogen cycles. Then 50 mg of fluorinated graphite was added to the DMF and sonicated for 4 h. In a 50 mL balloon, 4 g of potassium carbonate and 2 mL of diethylmalonate were dissolved in 7.5 mL of DMF at 130 °C, and the resulting solution was stirred for 1 h at 0 °C. This solution was then combined with the fluorinated graphite suspension and allowed to react at 130 °C for 24 h. The resulting suspension was filtered on a PTFE membrane and washed with 100 mL of DMF, 100 × 2 mL of acetone, and finally with 100 × 3 mL of water on a PC membrane. The product obtained is dispersed in 100 mL of water at pH ≈3 with HCl and sonicated for 1 h. The resulting suspension was kept at reflux for 24 h, then filtrated on a PC membrane and

washed with water until neutrality. Finally, the obtained solid compound was washed with 100×3 mL of acetone and left to dry.

Morphological and Chemico-Physical Characterizations:

(a) Transmission electron microscopy (TEM): Transmission electron microscope (TEM) images were recorded with a FEI Tecnai G2 equipped with a side-mounted Olympus Veleta camera and a bottom-mounted TVIPS F114 camera.

(b) Scanning electron microscopy (SEM): SEM imaging was performed by using a field emission source equipped with a GEMINI column (Zeiss Supra VP35) and micrographs were obtained with an acceleration voltage of 5 or 10 kV using in-lens high-resolution detection.

(c) Thermal analysis: Thermogravimetric analyses were carried out with Q5000IR TGA (TA Instruments) under nitrogen by an isotherm at 50 °C for 15 min followed by heating at 10 °C min^{-1} until 800 °C

(d) Infrared spectroscopy: Solid-state Fourier Transform Infrared (FT-IR, KBr disk technique) absorption spectra were recorded with a Nicolet Nexus FT-IR spectrometer.

(e) Raman spectroscopy: The Raman spectra were collected using a ThermoFisher DXR Raman microscope using a laser source with an excitation wavelength of 532 nm (1 mW), focused on the sample with a 50× objective (Olympus).

(f) X-ray photoelectron spectroscopy: The GAA samples were suspended in 2-propanol and drop-casted on a Cu metal substrate. The chemical analysis has been carried out using a custom-made UHV system working at a base pressure of 10^{-10} mbar, equipped with an Omicron EA125 electron analyzer and an Omicron DAR 400 X-ray source with a dual Al-Mg anode. Core level photoemission spectra (C 1s, N 1s, O 1s, F 1s, and Fe 2p) were collected at RT with a non-monochromatic Al Kα X-ray source (1286.6 eV) and using an energy step of 0.1 eV, 0.5 s of integration time, and 20 eV of pass energy.

(g) Profilometry: The GAA samples were analyzed by using a KLA Tencor P-17 profilometer with a tip radius of 2 µm.

(h) ζ-Potential analysis: ζ-potential measurements were carried out on Malvern Panalytical Zetasizer Nano ZS90 using 0.1 mg mL^{-1} suspensions of N-Gr in water.

GAA-Based Supercapacitor:

(a) Four-Point Probe measurements: Electrical conductivity measurements were conducted on pelletized samples: 50 mg of GAA were pressed under 10 tons with a Specac press machine. The electrical resistivity was measured with Jandel, Model RM3000, featuring a limit of detection 10^7 W sq^{-1}. The electrical conductivity (σ) was obtained as:

$$\sigma = \frac{1}{(R_s \cdot l)} \tag{2}$$

where *Rs* is the sheet resistance and $l = 0.64$ mm is the thickness of the electrode.[69,70]

(b) Electrode fabrication: The stepwise manufacturing of the electrodes proceeded as follows. First, a paste was prepared by fully mixing 90 wt% of the sample (18 mg), 10 wt% of polytetrafluoroethylene (PTFE) binder (2 mg), and a certain amount of NMP using an agate mortar and pestle. The paste was coated over the carbon paper electrode, which was then subjected to a quick dry at 80 °C. The electrodes were completely dried at 80 °C in a vacuum oven for 16 h. The mass loading of the GAA was ~1 mg in each electrode.

(c) Fabrication of symmetric supercapacitors: The electrochemical performance of the GAA was measured in a two-electrode symmetric supercapacitor system. Two electrodes were assembled in CR2032 stainless steel coin-type cells with a porous cellulose membrane as separator and 6 M KOH aqueous solution as electrolyte.

(d) Fabrication of zinc hybrid supercapacitors (Zn-HSCs): Zinc foil was directly used as an anode electrode after being polished with gauze and pouched into electrodes with a 12 mm diameter. Zn foil anode and our electrode material as cathode were assembled in CR2032 stainless steel coin-type cells with a porous cellulose membrane as separator and 2 M Zinc trifluoromethanesulfonate ($Zn(OTf)_2$) aqueous solution as electrolyte.

(e) Electrochemical characterization: The devices were electrically characterized by cyclic voltammetry (CV), galvanostatic charge/discharge (GCD), and electrochemical impedance spectroscopy (EIS) employing a Metrohm Autolab PGSTAT204 potentiostat/galvanostat and the Autolab DuoCoin Cell Holder (Metrohm AG). The frequency range for the impedance spectra was from 0.1 Hz to 100 kHz with a sine-wave voltage signal amplitude of 50 mV (root-mean-square, RMS). The CV and GCD tests were carried out between 0 and 1 V for supercapacitors and between 0 and 1.8 V for Zn-HSCs. The stability tests were performed employing a Battery Testing System (Neware).

(f) Electrochemical calculations:

i. *Calculation of the gravimetric capacitances*: The gravimetric capacitance was calculated using GCD with the following equation:

$$C_s = \frac{2 \cdot I \cdot \Delta t}{\Delta V \cdot m} \tag{3}$$

where, I (A) is the response current, Δt (s) is the discharge time, ΔV (V) is the voltage window, and m (g) is the mass of GAA in a single electrode.

ii. *Power and energy density calculations*: The energy density of the device was obtained from the formula:

$$E = \frac{1}{2} \cdot C \cdot \frac{(\Delta V)^2}{3.6} \tag{4}$$

The power density of the device was calculated from the formula:

$$P = \frac{E}{\Delta t} \cdot 3600 \tag{5}$$

where E is the specific energy (Wh kg^{-1}), C is the gravimetric capacitance (F/g), ΔV is the potential window (V), P is the power density (W kg^{-1}) and Δt is the discharge time (s).

iii. *Calculation of ionic conductivity (σ)*: The ionic conductivity was calculated as:

$$\sigma = \frac{l}{R \cdot A} \tag{6}$$

where σ is the ionic conductivity (S m^{-1}), l is the film thickness (m), A is the contact area (m^2), and R (Ω) is the total resistance of the electrolyte sample that was obtained from the Nyquist plot of complex impedance measurements. The value of R employed for the ionic conductivity calculation is equal to R_{ct} as described in the literature.[50,71] The film thickness was determined by SEM cross-section measurements, and it amounted to 100 µm. The area of the electrode can be directly determined from its diameter, and it amounted to 1.27 cm^2.

GAA-Based LGT:

a) Devices preparation: We fabricated liquid-gated GAA-based transistors onto Au micro-electrodes prepared by standard photolithography onto Si/SiO_2 substrates. These devices comprise Au interdigitated electrodes (IDEs) with a gap of 30 µm and a coplanar Au square 3×3 mm^2 gate.

The synthesized GAA was diluted in Milli-Q water in the proportion of 1 mg mL^{-1} and 5 mg mL^{-1}. For the GAA deposition, we exploited the

spontaneous adsorption of polyelectrolytes with drop-casting. As both GAA dispersion and the Si/SiO_2 surface are negatively charged, before GAA deposition, we immersed the substrate in a PDDA solution, 1% w/w, and 0.5 M NaCl, for 15 minutes. This procedure created an adhesive layer to promote GAA adhesion. After a careful rinse with bi-distilled water, we cast a GAA droplet (10-20 µl) onto the previously formed PDDA layer. Moreover, to increase the amount of GAA in order to achieve electrical conductivity, we exploited drop-casting deposition. Optimization of the deposition process proved the necessity to control the drying process. To achieve this, the substrates were placed in a plastic petri dish and a few droplets of 1% N-methyl-2-pyrrolidone (NMP) solution in Milli Q water (v/v) were placed onto the Si/SiO_2 substrates before GAA deposition. Then, the petri dish was kept closed until the GAA droplet was completely dried. A similar procedure has already been reported to avoid "coffee rings" formation during the inkjet printing of gold nanoparticles,[72] and the deposition of [1]benzothieno[3,2-b][1]-benzothiophene-peptide hydrogels.[73]

Usually, organic field-effect transistors (OFETs) are based on an ultra-thin organic semiconductor layer onto the channel. Therefore, the GAA 1 mg mL^{-1} at pH 10 was deposited onto the IDEs, in which the drop-casting procedure was repeated three times. Moreover, to increase the gate capacitance, GAA 5 mg mL^{-1} was drop-cast onto the Au square. Two different droplets of Nafion 117 (~ 5% in a mixture of lower aliphatic alcohols and water) were spin-coated at 2000 rpm for 1 minute onto the GAA channel and GAA-coated gate terminal to avoid any detachment of the GAA layers once immersed in aqueous solution and to stabilize the device. A sketch of the produced GAA-LGT is shown in Figure 3a.

b) LGT characterization: All measurements were performed in 0.1 M NaCl, keeping the devices in a Faraday cage.

For the LGT characterization, an Agilent B1500 parameter analyser was used, equipped with two high-power and two high-resolution source measurement units (SMUs). The I-V curves were interpreted according to the convention introduced by Lago et al.,[43,61] to describe ambipolar LGTs. So, each comb of the IDEs corresponds to the positive (P) and negative (N) terminals (i.e., $V_P \geq 0$ V, and $V_N < 0$ V), which act as holes-source/electrons-drain and electrons-source/holes-drain, respectively.[43,61] Consequently, I_P and I_N are the currents measured on the P and N terminals. In our case, the P electrode is the common terminal for both gate and N ones and is always grounded, i.e., $V_P = 0$ V.

To investigate the response time, high V_G square pulses (i.e., $|\Delta V_G| > 100$ mV) were applied to the GAA-coated gate. In this configuration, the V_G potential switches from the one related to the lowest to the highest transconductances ($\frac{\partial I_P}{\partial V_G}$), lasting 60 s. Moreover, to assess the potentiometric sensitivity, V_G steps lower than 20 mV were applied on the GAA-coated gate for 60 seconds to investigate the smallest detectable potential change in the electrolyte.

Prolonged electrical stress was investigated by using a lab paper to drive 0.1 M NaCl onto our GAA-LGT. The characterization relied on recording the current of our GAA-LGT as a function of time by fixing V_N = -300 mV, $V_P = 0$ V, and $V_G = +250$ mV or $V_G = -300$ mV.

Supporting Information

Supporting Information is available from the Wiley Online Library or from the author.

Acknowledgements

S.C. acknowledges the financial support from the Italian Ministry of Education, Universities, and Research through the project "Nanochemistry for Energy and Health, NexuS"—the national funding network termed "Dipartimenti di Eccellenza" awarded to the Department of Chemical Sciences at the University of Padua and the project P-DiSC#11NexuS_BIRD2020-UNIPD (CARBON-FET). S.C. and G.G.I. acknowledge the research grant "Bando Vinci 2021" funded by the Italian-French University. R.C.H. acknowledges the research grant no. 2020/15095-0 from São Paulo Research Foundation – FAPESP (Brazil). The activity in Strasbourg was financially supported by the European Commission through ERC project SUPRA2DMAT (GA-833707), the Graphene Flagship Core 3 project (GA-881603) as well as the Agence Nationale de la Recherche through the Interdisciplinary Thematic Institute SysChem via the IdEx Unistra (ANR-10-IDEX-0002) within the program Investissement d'Avenir, the Fondation Jean-Marie Lehn, the Institut Universitaire de France (IUF).

Conflict of Interest

The authors declare no conflict of interest.

Data Availability Statement

The data that support the findings of this study are available from the corresponding author upon reasonable request.

Keywords

2D materials, graphene-related materials, liquid-gated transistors, supercapacitors, Graphene acid

Received: October 6, 2023
Revised: December 28, 2023
Published online: January 16, 2024

[1] M. C. Lemme, T. J. Echtermeyer, M. Baus, H. Kurz, *IEEE Electron Device Lett.* **2007**, *28*, 282.
[2] P. Avouris, *Nano Lett.* **2010**, *10*, 4285.
[3] Y. Zhang, Y.-W. Tan, H. L. Stormer, P. Kim, *Nature* **2005**, *438*, 201.
[4] K. S. Novoselov, A. K. Geim, S. V. Morozov, D. Jiang, Y. Zhang, S. V. Dubonos, I. V. Grigorieva, A. A. Firsov, *Science 1979* **2004**, *306*, 666.
[5] C. I. Idumah, *Emergent Mater.* **2023**, *6*, 777.
[6] S. K. Krishnan, N. Nataraj, M. Meyyappan, U. Pal, *Anal. Chem.* **2023**, *95*, 2590.
[7] C. Dai, D. Kong, C. Chen, Y. Liu, D. Wei, *Adv. Funct. Mater.* **2023**, *n/a*, 2301948.
[8] G. F. Smaisim, A. M. Abed, H. Al-Madhhachi, S. K. Hadrawi, H. M. M. Al-Khateeb, E. Kianfar, *J. Bionanosci.* **2023**, *13*, 219.
[9] A. P. Singh, P. N. Shankar, R. Baghel, S. Tirkey, in *2023 IEEE Int. Students' Conf. on Electrical, Electronics and Computer Science (SCEECS)*, IEEE, Piscataway, NJ **2023**, pp. 1.
[10] C. Backes, A. M. Abdelkader, C. Alonso, A. Andrieux-Ledier, R. Arenal, J. Azpeitia, N. Balakrishnan, L. Banszerus, J. Barjon, R. Bartali, S. Bellani, C. Berger, R. Berger, M. M. B. Ortega, C. Bernard, P. H. Beton, A. Beyer, A. Bianco, P. Bøggild, F. Bonaccorso, G. B. Barin, C. Botas, R. A. Bueno, D. Carriazo, A. Castellanos-Gomez, M. Christian, A. Ciesielski, T. Ciuk, M. T. Cole, J. Coleman, et al., *2D Mater.* **2020**, *7*, 022001.
[11] R. Taira, A. Yamanaka, S. Okada, *Appl. Phys. Express* **2016**, *9*, 115102.
[12] A. Criado, M. Melchionna, S. Marchesan, M. Prato, *Angew. Chem., Int. Ed.* **2015**, *54*, 10734.
[13] T. S. Sreeprasad, V. Berry, *Small* **2013**, *9*, 341.
[14] P. Plachinda, D. Evans, R. Solanki, *AIMS Mater. Sci.* **2017**, *4*, 340.
[15] X. Ming, *E3S Web Conf.* **2021**, *231*, 01007.
[16] E. Mazarei, C. Penschke, P. Saalfrank, *ACS Omega* **2023**, *8*, 22026.
[17] H. Zhang, E. Bekyarova, J.-W. Huang, Z. Zhao, W. Bao, F. Wang, R. C. Haddon, C. N. Lau, *Nano Lett.* **2011**, *11*, 4047.

[18] E. Aliyev, V. Filiz, M. M. Khan, Y. J. Lee, C. Abetz, V. Abetz, *Nanomaterials* **2019**, *9*, 1180.
[19] A. H. De Lima, I. Scarpa, N. C. L. Azevedo, G. C. Lelis, M. Strauss, D. S. T. Martinez, R. Furlan De Oliveira, *J. Mater. Chem. C* **2023**, *11*, 12429.
[20] C. Gómez-Navarro, R. T Weitz, A. M. Bittner, M. Scolari, A. Mews, M. Burghard, K. Kern, *Nano Lett.* **2007**, *7*, 3499.
[21] Y.-L. Zhang, Li Guo, H. Xia, Q.-D. Chen, J. Feng, H-B. Sun, *Adv. Opt. Mater.* **2014**, *2*, 10.
[22] R. Trusovas, K. Ratautas, G. Raciukaitis, J. Barkauskas, I. Stankeviciene, G. Niaura, R. Mazeikiene, *Carbon N Y* **2013**, *52*, 574.
[23] Y. Zhou, Q. Bao, L. A. L. Tang, Y. Zhong, K. P. Loh, *Chem. Mater.* **2009**, *21*, 2950.
[24] D. Voiry, J. Yang, J. Kupferberg, R. Fullon, C. Lee, H. Y. Jeong, H. S. Shin, M. Chhowalla, *Science* **2016**, *353*, 1413.
[25] J. M. Mativetsky, A. Liscio, E. Treossi, E. Orgiu, A. Zanelli, P. Samorì, V. Palermo, *J. Am. Chem. Soc.* **2011**, *133*, 14320.
[26] A. C. Faucett, J. N. Flournoy, J. S. Mehta, J. M. Mativetsky, *FlatChem* **2017**, *1*, 42.
[27] M. C. Morant-Miñana, J. Heidler, G. Glasser, H. Lu, R. Berger, N. Gil-Gonzalez, K. Müllen, D. M. De Leeuw, K. Asadi, *Mater. Horiz.* **2018**, *5*, 1176.
[28] D. D. Chronopoulos, A. Bakandritsos, M. Pykal, R. Zboril, M. Otyepka, *Appl. Mater. Today* **2017**, *9*, 60.
[29] H. Sun, T. Li, F. Lei, M. Yang, D. Li, X. Huang, D. Sun, *Polym. Int.* **2020**, *69*, 457.
[30] A. Bakandritsos, M. Pykal, P. Blonski, P. Jakubec, D. D. Chronopoulos, K. Poláková, V. Georgakilas, K. Cpe, O. Tomanec, V. Ranc, A. B. Bourlinos, R. Zboril, M. Otyepka, *ACS Nano* **2017**, *11*, 2982.
[31] Yi Heng Cheong, M. Z. M. Nasir, A. Bakandritsos, M. Pykal, P. Jakubec, R. Zboril, M. Otyepka, M. Pumera, *ChemElectroChem* **2019**, *6*, 229.
[32] S. Mohammadi, S. M Mousavi-Khoshdel, *Sci. Rep.* **2023**, *13*, 16756.
[33] W. Czepa, S. Witomska, P. Samorì, A. Ciesielski, *Small Sci.* **2023**, *3*, 2300013.
[34] E. C. Vermisoglou, P. Jakubec, A. Bakandritsos, V. Kupka, M. Pykal, V. Sedajová, J. Vlcek, O. Tomanec, M. Scheibe, R. Zboril, M. Otyepka, *ChemSusChem* **2021**, *14*, 3904.
[35] G. Sun, Y. Xiao, B. Lu, X. Jin, H. Yang, C. Dai, X. Zhang, Y. Zhao, L. Qu, *ACS Appl. Mater. Interfaces* **2020**, *12*, 7239.
[36] H. Du, Xi Lin, Z. Xu, D. Chu, *J. Mater. Sci.* **2015**, *50*, 5641.
[37] L. Kergoat, L. Herlogsson, B. Piro, M. C. Pham, G. Horowitz, X. Crispin, M. Berggren, *Proc. Natl. Acad. Sci. USA* **2012**, *109*, 8394.
[38] C. Reiner-Rozman, M. Larisika, C. Nowak, W. Knoll, *Biosens. Bioelectron.* **2015**, *70*, 21.
[39] E. Piccinini, C. Bliem, C. Reiner-Rozman, F. Battaglini, O. Azzaroni, W. Knoll, *Biosens. Bioelectron.* **2017**, *92*, 661.
[40] R. Furlan De Oliveira, P. A. Livio, V. Montes-García, S. Ippolito, M. Eredia, P. Fanjul-Bolado, M. B. González García, S. Casalini, P. Samorì, *Adv. Funct. Mater.* **2019**, *29*, 1905375.
[41] S. Vasilijevic, G. Mattana, G. Anquetin, N. Battaglini, B. Piro, *Electrochim. Acta* **2021**, *371*, 137819.
[42] R. C. Hensel, N. Comisso, M. Musiani, F. Sedona, M. Sambi, A. Cester, N. Lago, S. Casalini, *J. Mater. Chem. C* **2023**, *11*, 8876.
[43] N. Lago, M. Buonomo, R. C. Hensel, F. Sedona, M. Sambi, S. Casalini, A. Cester, *IEEE Trans. Electron Devices* **2022**, *69*, 3192.
[44] M. Sensi, R. F. De Oliveira, M. Berto, M. Palmieri, E. Ruini, P. A. Livio, A. Conti, M. Pinti, C. Salvarani, A. Cossarizza, J. M. Cabot, J. Ricart, S. Casalini, M. B. González-García, P. Fanjul-Bolado, C. A. Bortolotti, P. Samorì, F. Biscarini, *Adv. Mater.* **2023**, *35*, 2211352.
[45] V. Šedajová, P. Jakubec, A. Bakandritsos, V. Ranc, M. Otyepka, *Nanomaterials* **2020**, 10.
[46] T. Cramer, A. Campana, F. Leonardi, S. Casalini, A. Kyndiah, M. Murgia, F. Biscarini, *J. Mater. Chem. B* **2013**, *1*, 3728.
[47] F. Chen, Q. Qing, J. Xia, J. Li, N. Tao, *J. Am. Chem. Soc.* **2009**, *131*, 9908.
[48] B. J. Kim, M. S. Kang, V. H. Pham, T. V. Cuong, E. J. Kim, J. S. Chung, S. H. Hur, J. Ho Cho, *J. Mater. Chem.* **2011**, *21*, 13068.
[49] E. Frackowiak, F. Béguin, *Carbon N Y* **2001**, *39*, 937.
[50] P. Vadhva, J. Hu, M. J. Johnson, R. Stocker, M. Braglia, D. J. L. Brett, A. J. E. Rettie, *ChemElectroChem* **2021**, *8*, 1930.
[51] D. Pakulski, V. Montes-García, A. Gorczynski, W. Czepa, T. Chudziak, P. Samorì, A. Ciesielski, *J. Mater. Chem. A Mater.* **2022**, *10*, 16685.
[52] C. Byoung-Yong, *J. Electrochem. Sci. Technol.* **2020**, *11*, 318.
[53] E. C. Vermisoglou, P. Jakubec, A. Bakandritsos, M. Pykal, S. Talande, V. Kupka, R. Zboril, M. Otyepka, *Chem. Mater.* **2019**, *31*, 4698.
[54] O. Jankovský, M. Nováček, J. Luxa, D. Sedmidubský, V. Fila, M. Pumera, Z. Sofer, *Chemistry* **2016**, *22*, 17416.
[55] Z. Wang, Z. Hao, X. Wang, C. Huang, Q. Lin, X. Zhao, Y. Pan, *Adv. Funct. Mater.* **2021**, *31*, 2005958.
[56] S. J. Lue, Y.-L. Pai, C.-M. Shih, M.-C. Wu, S.-M. Lai, *J. Memb. Sci.* **2015**, *493*, 212.
[57] P.-P. Lu, D.-S. Shang, C.-S. Yang, Y. Sun, *J. Phys. D Appl. Phys.* **2020**, *53*, 485102.
[58] N. F. Sheppard, R. C. Tucker, C. Wu, *Anal. Chem.* **1993**, *65*, 1199.
[59] T. Xiao, X. Song, *J. Chem. Phys.* **2011**, *135*, 104104.
[60] M. Singh, K. Manoli, A. Tiwari, T. Ligonzo, C. Di Franco, N. Cioffi, G. Palazzo, G. Scamarcio, L. Torsi, *J Mater Chem C Mater* **2017**, *5*, 3509.
[61] N. Lago, M. Buonomo, R. C. Hensel, F. Sedona, M. Sambi, S. Casalini, A. Cester, *IEEE Trans. Electron Devices* **2022**, *69*, 6492.
[62] A. Mathkar, D. Tozier, P. Cox, P. Ong, C. Galande, K. Balakrishnan, A. Leela Mohana Reddy, P. M. Ajayan, *J. Phys. Chem. Lett.* **2012**, *3*, 986.
[63] K.-Y. Lian, Y.-F. Ji, X.-F. Li, M.-X. Jin, D.-J. Ding, Y. Luo, *J. Phys. Chem. C* **2013**, *117*, 6049.
[64] E. Danielson, V. A. Sontakke, A. J. Porkovich, Z. Wang, P. Kumar, Z. Ziadi, Y. Yokobayashi, M. Sowwan, *Sens Actuators B Chem* **2020**, *320*, 128432.
[65] R. Furlan De Oliveira, V. Montes-García, P. A. Livio, M. B. González-García, P. Fanjul-Bolado, S. Casalini, P. Samorì, *Small* **2022**, *18*, 2201861.
[66] P. Servati, D. Striakhilev, A. Nathan, *IEEE Trans. Electron Devices* **2003**, *50*, 2227.
[67] N. Lago, in *2022 14th Int. Conf. on Advanced Semiconductor Devices and Microsystems (ASDAM)*, Smolenice, Slovakia, October **2022**.
[68] G. C. Faria, D. T. Duong, A. Salleo, *Org. Electron.* **2017**, *45*, 215.
[69] S. Yilmaz, *J. Semicond.* **2015**, *36*.
[70] B. Jafari, C. M. R. Lacerda, G. G. Botte, *ChemElectroChem* **2023**, *10*, 202201111.
[71] R. A. Huggins, *Ionics* **2002**, *8*, 300.
[72] E. Chow, J. Herrmann, C. S. Barton, B. Raguse, L. Wieczorek, *Anal. Chim. Acta* **2009**, *632*, 135.
[73] A. Fortunato, R. C. Hensel, S. Casalini, M. Mba, *Molecules* **2023**, *28*, 2917.